CONF-951155--21

LA-UR-95- 4194

Title: DIRECTED LIGHT FABRICATION OF IRON-BASED MATERIALS

Author(s): Dan J. Thoma, MST-6
Gary K. Lewis, MST-6
Ronald B. Nemec, MST-6
Christian Charbon, CMS

Submitted to: MRS Fall Meeting '95,
Symp. B- Advanced Laser Processing of Materials-Fundamental's and Application
November 27-December 1, 1995

Los Alamos
NATIONAL LABORATORY

Form No. 836 R5
ST 2629 10/91

DIRECTED LIGHT FABRICATION OF IRON-BASED MATERIALS

D.J. Thoma, C. Charbon, G.K. Lewis, and R.B. Nemec
Los Alamos National Laboratory, Mail Stop G770, Los Alamos, NM 87545

ABSTRACT

Directed light fabrication (DLF) is a process that fuses gas delivered metal powders within a focal zone of a laser beam to produce fully dense, 3-dimensional metal components. From a computer generated solid model, deposition "tool paths" are constructed that command the laser movement to fabricate near net shape parts a layer at a time. Among potential candidate systems to study, iron-based alloys are particularly attractive for rapid prototyping. To evaluate the processing parameters in the DLF process, studies have been performed on the microstructural development in 1-dimensional and 2-dimensional Fe-based components. For example, continuous microstructural features are evident, implying a continuous liquid/solid interface during processing. In addition, solidification cooling rates have been determined based upon secondary dendrite arm spacings in Fe-25wt.%Ni and 316 stainless steel. Cooling rates vary from 10^1-10^5 K s^{-1}, and the solidification behavior has been simulated using macroscopic heat transfer analyses.

INTRODUCTION

Directed light fabrication (DLF) is a rapid prototyping process that fuses gas-delivered metal powders within a focal zone of a laser beam to produce 3-dimensional metal components [1]. The focal zone of the laser beam is programmed to move along or across a part cross-section, and coupled with a multi-axis sample stage, produces complex metal geometries. The DLF process yields a final geometry from a single piece of equipment operating under the appropriate software control.

Potential metal rapid prototyping processes include liquid metal spraying, plasma spraying, electron beam vapor deposition, and investment casting processes. These metal processing techniques, unlike the DLF process, are non-directional deposition processes that require mold patterns or masks to gain the detail for complex parts and assemblies. Therefore, DLF processing offers unique capabilities and advantages for rapid prototyping of complex metal components. Initial candidate alloy systems for rapid prototyping include iron-based materials. In order to define and optimize the processed materials, an examination of the microstructural development is required. The microstructural development in steels affect the mechanical properties of the material, and in particular, the thermal history of fabricated components dictates the potential application. The intent of this study is to address the solidification behavior with a specific focus upon the cooling rates experienced during DLF processing of simple geometries.

PROCEDURE

Experimental

The DLF process consists of generating tool paths from computer generated 3-dimensional solid models. The tool paths continuously move the focal zone of the laser systematically along areas of the part to fuse metal powder particles that are gas-delivered to the focal zone. A schematic diagram of the process is shown in Figure 1. Three Nd-YAG pulsed lasers (1 KW),

connected in series to simulate a continuous wave (CW) laser beam, are delivered via fiber optics to a sealed boom that holds the laser focusing head and is attached to the "z" (vertical) axis. The focused laser beam enters the chamber through a quartz window in a nozzle that also delivers the metal powder to the focal zone. The entire process takes place in an inert gas box connected to a dry train that reduces the oxygen content to < 5 ppm. In the upper right of the schematic diagram is a chamber that can be evacuated and back-filled with an inert gas that contains the powder feeder. The powder feeder entrains the powder in an argon stream that delivers the powder to the laser focus nozzle and then to the focal zone. A positioning controller drives the "x", "y", and "z" tables, switches the laser shutter and powder feeder on and off, and controls the gas flow.

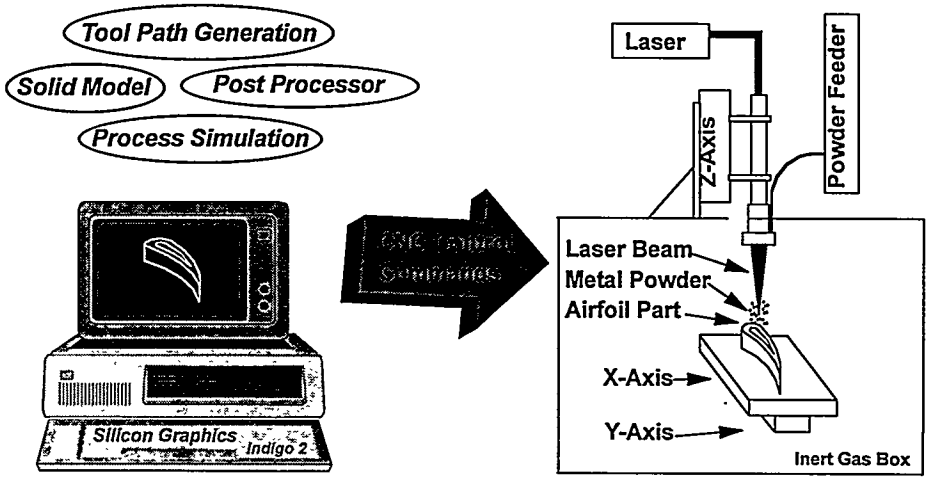

Figure 1 - Schematic diagram of the DLF process

For the purpose of evaluating the solidification behavior in DLF, 1-dimensional and 2-dimensional experimental studies were conducted. The 1-dimensional studies consisted of only z-direction growth of rods (~40 mm long and 3 mm in diameter). Plates (or walls) were produced for the 2-dimensional study by building up horizontal layers of continuously fused powder. The walls typically have dimensions of 25 mm x 40 mm x 3 mm (length x height x width). The materials explored were Fe-24.8wt.%Ni and 316 stainless steel. All starting powders were approximately 50 μm in diameter and were commercially available.

Computational

A simple one dimensional (1D) finite difference model aimed at describing the temperature evolution of a growing rod has been developed. The model accounts for the growth of the rod, the heat conduction through the rod, the heat losses by radiation at the surface of the rod, the heat flux generated by the laser beam at the top of the rod, and for the heat flux generated by the cooling chill at the base of the rod.

It is considered that the rod of length l(t) expands at a constant speed, v_l. This speed is simply given by the final length of the rod, l_{end}, divided by the time used to grow it, Δt_g.

The differential equation to solve is the heat balance [2]:

$$\frac{\partial}{\partial z}\kappa\frac{\partial T}{\partial z}=\frac{\partial H}{\partial t}-v(z)\frac{\partial H}{\partial z} \qquad (1)$$

where z is the position, k the thermal conductivity, T the temperature, H the volumetric enthalpy and t the time. The velocity, v(z), which appears on the right hand side of Eq. 1 is a linear function of the position, z. The velocity evolves from 0 at the base of the rod to v_l at the top of

the rod. This advection-like term accounts for the fact that, over time, the nodes are moving through a temperature gradient.

The boundary condition at the top of the rod, is a Neuman-type condition. A constant heat flux, q_l, is imposed. Although this quantity is unknown, it is a fraction of the nominal power of the laser divided by the cross section of the rod. Energy is lost by reflection and by heating particles of the powder which are not included in the growth of the rod.

The boundary condition at the bottom of the rod is a Cauchy-type condition.

$$q_h = h(T_c - T_b) \tag{2}$$

The heat flux, q_h, is proportional to the difference between the temperature at the base of the rod, T_b, and the temperature of the cooling chill, T_c. In the present model, the heat transfer coefficient, h, is supposed to be a constant. The temperature of the cooling chill is taken as an exponentially decreasing function of time.

Radiation is accounted for by applying a heat flux, q_r, to each node which is equal to:

$$q_r = \sigma\varepsilon\left(T_a^4 - T^4\right) = \sigma\varepsilon\left(T_a^3 - T_a^2 T + T_a T^2 + T^3\right)(T_a - T) = h_{rad}(T_a - T) \tag{3}$$

where σ is the Boltzmann constant, ε the emissivity and T_a the ambient temperature. This heat flux is applied to the lateral surface of the rod which introduces a new variable in the definition of the problem: the radius of the rod, r.

The formulation in finite differences has been made in an implicit way, except for the radiation term which is expressed in a semi-explicit way. The radiative heat-flux is transformed in a Cauchy-type heat flux where the radiative heat transfer coefficient, h_{rad}, is determined explicitly from the temperature at the previous time step whereas the temperature difference is taken implicitly. The final formulation of the problem is a system of equations which may be written as:

$$[A]\vec{T}^{t+\Delta t} + [B]\vec{H}^{t+\Delta t} + \vec{C} = \vec{0} \tag{4}$$

where [A] and [B] are two tri-diagonal matrixes. Iterations are necessary in order to solve this system which is non linear, due to the non linear relationship between T and H and the temperature dependence of the thermal conductivity. The temperature vector is eliminated by a first order linearisation of the T=T(H) relationship (Newton's method) and the system is solved by a tridiagonal matrix algorithm (TDMA).

The relationship between temperature and enthalpy is deduced from the enthalpy definition: :

$$H(T) = \int_0^T c_p(\theta)\,d(\theta) + \left(1 - f_s(T)\right) \tag{5}$$

where c_p is the volumetric specific heat, L the volumetric latent heat and f_s the volumetric fraction of solid. The solidification path, $f_s=f_s(T)$, is given by Scheil's model [$$].

RESULTS AND DISCUSSION

Solid/Liquid Interface

A longitudinal cross-section of a 316 stainless steel rod processed by DLF is shown in Figures 2a. The rod has continuous dendrites along the length of the sample. Since the microstructural development in the DLF processed sample displays continuous morphologies, a constant solid/liquid interface must be maintained. A schematic diagram of the rod growth process is shown in Figure 2b. Apparently, a molten layer of the alloy resides at the top of the rod, and the solid dendrites continuously grow (in the mushy zone) during the process. Of course, if the molten zone is too large or too small, the stability and integrity of the process

decreases. Therefore, the processing variables, such as laser power, beam speed, and powder feed rate, are critical in producing uniform samples.

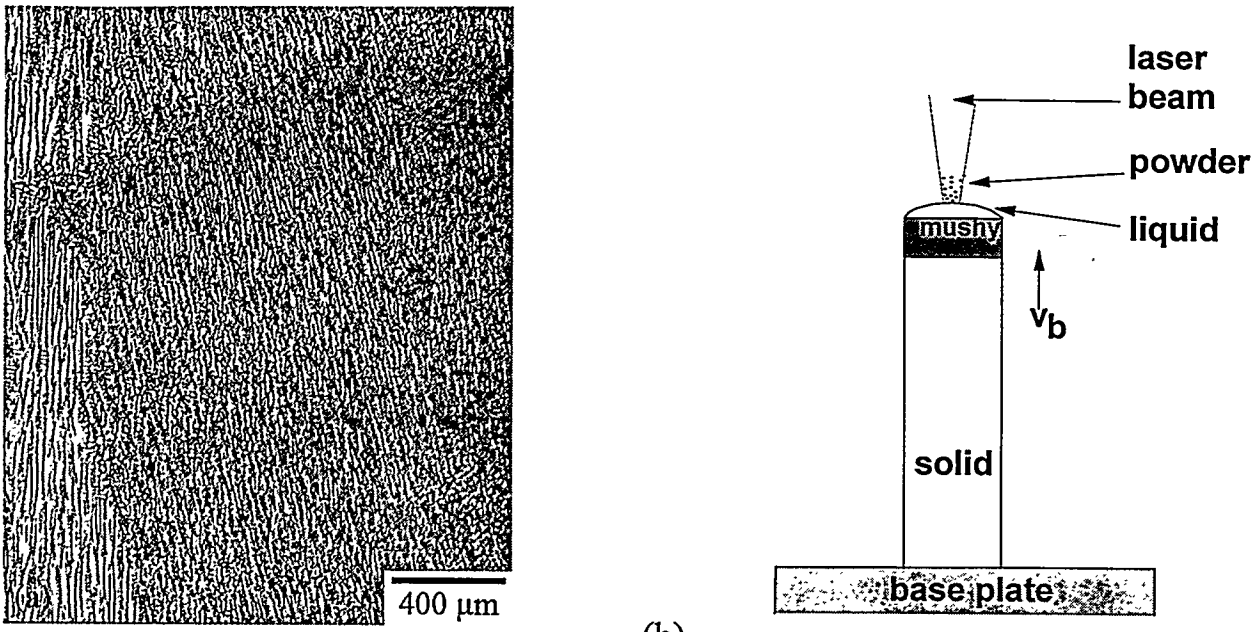

Figure 2 - (a) Cross-section micrograph of 316 stainless steel showing continuous dendrites, and (b) a schematic diagram of the processing of a rod

A longitudinal cross-sections of a 316 stainless steel plate sample is shown in Figure 3a, and a schematic diagram of the plate growth is shown in Figure 3b. As with the rod, the dendritic structure is continuous in the sample. Strong evidence of epitaxial growth off of the prior solid interface can be observed with each beam pass, and the zig-zag growth orientation of the layers results from the alternate processing directions of the multiple laser beam passes. In addition, a thin, heat-affected zone (~2 μm) is evident with each beam pass. In the schematic drawing of the plate growth, the mushy zone exists continuously, even at the corners of the plate, to maintain a constant solid/liquid interface. The continuous microstructural development in the plate growth supports the existence of the continuous solid/liquid interface during processing.

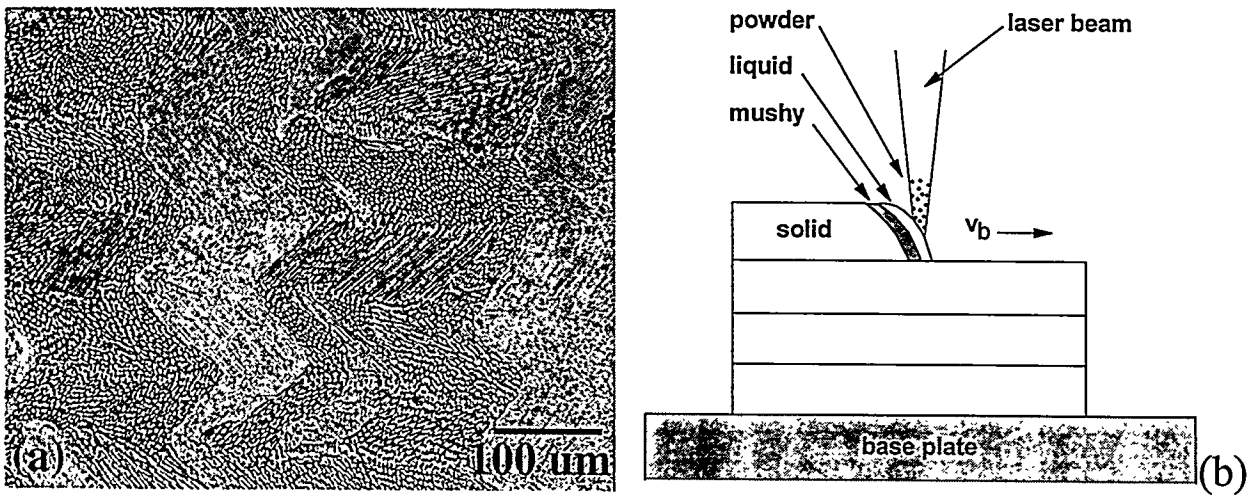

Figure 3 - (a) Cross-section of a 316 stainless steel wall, and (b) a schematic of the wall growth.

The continuous morphologies that result in DLF processing permit integrity in the mechanical properties. For example, DLF depositions result in mechanical properties that are equivalent to the annealed values. Tensile test results on 316 stainless steel plates show an average yield strength of 210 MPa, an ultimate strength of 485 MPa, 30% elongation, and a Youngs modulus of 210 GPa.

Cooling Rates

Secondary arm spacing analysis is a common technique to experimentally evaluate cooling rates during solidification [3]. Indeed, both empirical and theoretical studies have shown that the secondary dendrite arm spacing, λ_2, is related to the cooling rate, ε, by the relation

$$\lambda_2 = B\varepsilon^{-n} \tag{6}$$

where B is a constant and $n \cong 1/3$ [3

Empirical relationships relating the cooling rate to the secondary dendrite arm spacing have been well-documented for Fe-25wt.%Ni [4] and 316 stainless steel [5,6]. For Fe-25wt.%Ni, the relationship is

$$\lambda_2 = 60\varepsilon^{-0.32}. \tag{7}$$

The cooling rate has the units of (K/s) and λ_2 is expressed in microns. For 316 stainless steel, the empirical relationship is

$$\lambda_2 = 25\varepsilon^{-0.28}. \tag{8}$$

Both rods and plates of the two Fe-based alloys were grown by the DLF process, and example microstructures are shown in Figures 4a and 4b, respectively. The secondary arms spacings are indicated on the micrographs. For these two particular cases, secondary dendrite arm spacing in the rod was ~12.5 μm, and for the plate, λ_2 was ~3 μm. Therefore, the cooling rates were on the order of 150 K/s and $1x10^4$ K/s, respectively, for the rod and plate. Considering the qualitative changes in processing conditions, the cooling rates vary between 50-10^3 K/s for the rods and 10^3-10^5 K/s for the plates

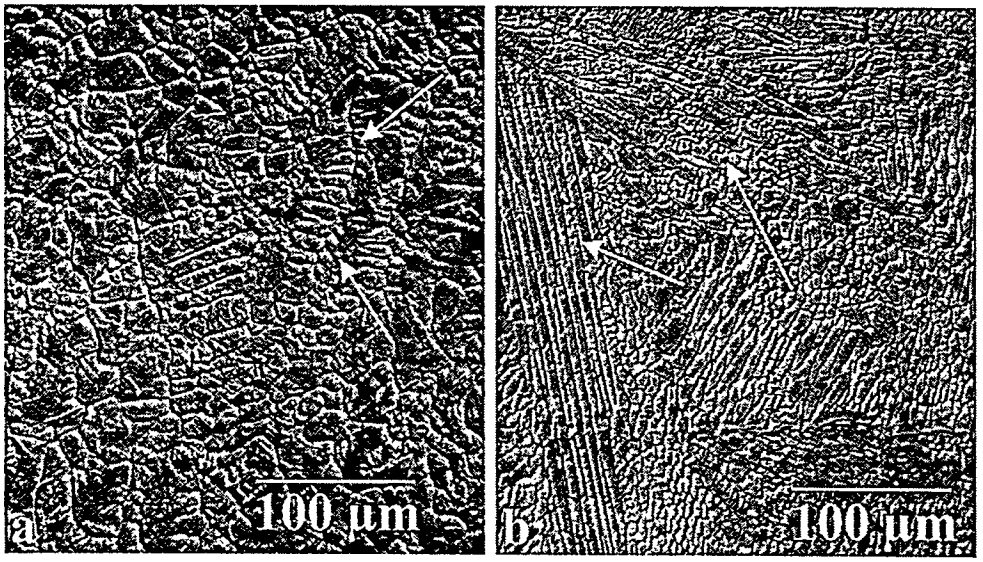

Figure 4 - Cross-section micrographs of an Fe-25wt.%Ni (a) rod, and (b) plate. Arrows indicate secondary dendrite arms

Calculations

A calculation has been performed with the data listed in Table I. The thermo-physical properties where taken from [7,8]. The output of the computer code is the evolution of the temperature field of the rod. The temperature profiles in the rod are plotted in Fig. 5a at different times. From these values, it is easy to determine such quantities as the thermal gradient, the cooling rate, the length of the mushy zone or any other quantity of interest.

The cooling rate and the thermal gradient at the azeotrope temperature are plotted on Fig.5b as a function of time.

Table I List of the parameters used in the computation.

l_0	10^{-6} m	r	1.5×10^{-3} m
l_{end}	3.91×10^{-2} m	Dt_g	42 s
v_1	9.31×10^{-4} ms^{-1}	q_1	10^7 Wm^{-2}
T_0	1300 °C	h	10^5 Wm^{-2}K^{-1}
T_a	25 °C	T_c	100+1400exp[-t/20] °C (t in s)
ε	0.8	N_n	1000

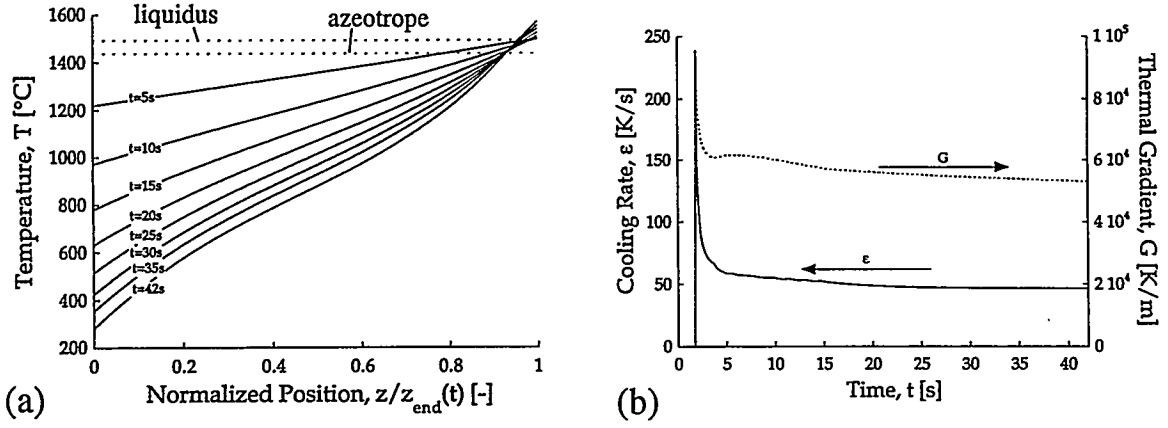

Figure 5 -

The cooling rate determined from the experimental measurement is equal to ~150 K/s whereas the cooling rate predicted by the model is equal to ~50 K/s. This discrepancy may be attributed to the large number of unknown parameters which are used in the model. However, the calculated value is certainly within the range of exerimentally determined values, and thermocouple measurements of the temperature in the cooling chill and at the surface of the rod are currently being evaluated to reduce the number of unknowns of the problem.

The simple thermal model developed in this study can be helpful to determine the solidification conditions during the DLF process. With the help of instrumented experiments, the model will develop into a predictive tool which will permit studies on the influence of process parameters on the solidification of a rod or a plate. As a result, a methodology will be developed to optimize the processing conditions.

ACKNOWLEDGMENTS

The research was funded under DOE Contract No. W-7405-ENG-36. The authors wish to thank Ann M. Kelly of Los Alamos National Laboratory (LANL) for metallographic preparations and Dr. Richard LeSar, Dr. Loren A. Jacobson and John O. Milewski (LANL) for useful interactions.

REFERENCES

1. Lewis, G.K., R.B. Nemec, J.O. Milewski, D.J. Thoma, M. Barbe, and D. Cremers, *Proc. ICALEO* (LIA, Orlando, FL) p. 17 (1994).
2. M. Rappaz, *Int. Mat. Reviews*, **34** p. 93 (1989)
3. Kurz, W. and D.J. Fisher, "Fundamentals of Solidification", 3rd ed., Trans Tech Publications, VT, (1989).
4. Brower, Jr., W.E., R. Strachan, and M.C. Flemings, *AFS Cast Metals Research Journal*, **Dec.**, p. 176, (1970).
5 Katayama, S. and A. Matsunawa, *Proc. ICALEO*, p. 60 (1984).
6. Elmer, J.W., S.M. Allen, and T.W. Eagar, *Metall. Trans. A*, **20A**, p. 2117, (1989).
7. Q. Zhao, T.J. Piccone, Y. Shiohara, and M.C. Flemings, Mater. Res. Soc. Symp. Proc., xxx p. (1988)
8. "ASM Handbook" xxth ed. vol. 1, (ASM